

Space Weather®



RESEARCH ARTICLE

10.1029/2022SW003134

Key Points:

- We present a machine learning model using global geomagnetic index/solar wind parameters to make topside electron density predictions at any location
- The wealth of available satellite data makes this well suited to machine learning, whereas current models of topside ionosphere are lacking
- This model has a correlation coefficient of 0.87 on testing data, and can outperform the International Reference Ionosphere at the high altitudes of the topside

Correspondence to:

S. Dutta, sdutta82@gatech.edu

Citation:

Dutta, S., & Cohen, M. B. (2022). Improving electron density predictions in the topside of the ionosphere using machine learning on in situ satellite data. *Space Weather*, 20, e2022SW003134. https://doi.org/10.1029/2022SW003134

Received 22 APR 2022 Accepted 29 JUL 2022

© 2022. The Authors. This is an open access article under the terms of the Creative Commons Attribution-NonCommercial License, which permits use, distribution and reproduction in any medium, provided the original work is properly cited and is not used for commercial purposes.

Improving Electron Density Predictions in the Topside of the Ionosphere Using Machine Learning on In Situ Satellite Data

S. Dutta¹ o and M. B. Cohen¹

¹School of Electrical and Computer Engineering, Georgia Institution of Technology, Atlanta, GA, USA

Abstract Modeling the Earth's ionosphere is a critical component of forecasting space weather, which in turn impacts radio wave propagation, navigation and communication. This research focuses on predicting the electron density in the topside of the ionosphere using satellite data, in particular from the Defense Meteorological Satellite Program, a collection of 19 satellites that have been polar orbiting the Earth for various lengths of times, fully covering 1982 to the present. An artificial neural network was developed and trained on two solar cycles worth of data (113 satellite-years), along with global drivers and indices such as F10.7, interplanetary magnetic field, and Kp to generate an electron density prediction. We tested the model on six years of subsequent data (26 satellite-years), and found a correlation coefficient of 0.87. Once trained, the model can predict topside electron density at any location specified by latitude and longitude given current/ recent geomagnetic conditions. We validated the model via comparison with data from the DEMETER satellite which orbited at a similar altitude, and taking that as an independent source of true electron density values. Comparing our results to the International Reference Ionosphere, we find that our model works better at low to mid-latitudes, and for quiet and moderately disturbed geomagnetic conditions, but not for highly disturbed conditions.

Plain Language Summary The sun interacts with the outer layers of the Earth's atmosphere. These interactions cause space weather, which like normal weather can be calm or stormy. A severe storm could cause widespread power outages and disrupt communication services. Unfortunately, we cannot predict space weather as well as we can predict normal weather. This work begins to solve this problem by developing a tool that can predict how the sun will impact one outer layer of the Earth's atmosphere, called the ionosphere. The tool combines data that is easier to measure directly and uses it to create these predictions, which we hope to eventually use as a part of an overall space weather forecasting system.

1. Introduction

The interaction of the sun with Earth's atmosphere and magnetic field can have potentially deleterious effects on Earth communication systems and power grids and can be better understood via space weather forecasting, and is therefore of interest to both Earth and space scientists as well as government and industry (Council, 2008). The topside ionosphere acts as the gateway between the lower F-region and the plasmasphere. During the day, the sun ionizes particles in the F-region, creating a swell of plasma into the plasmasphere, and at night, this plasma flows back down into the F-region. Understanding the mechanics of the topside ionosphere is crucial to creating a space weather forecast. Collecting electron density data from the topside is one way to further our understanding of the topside. However, typical ionospheric measurements are made with ground based ionosondes, which can only measure up to the bottomside of the F region. Surveying the electron density in specifically the topside of the ionosphere requires the data collection instrument to be located off of the ground, making more expensive sounders, radio occultation measurements, and probes on LEO satellites the only existing ways to get measurements of the topside (Pignalberi et al., 2018).

In this paper, we focus on ionospheric modeling based on in situ satellite data as a critical component of a space weather forecasting system, and look to improve upon the current standard empirical model, the International Reference Ionosphere (IRI) (Bilitza, 2018; Bilitza et al., 2017). The IRI provides a model of electron density, total electron content, ion and electron temperature, and ion drift over altitudes spanning 80–2,000 km, using sub-models for different altitude ranges. For example, the topside electron density predictions are made using R_{12} (the 12-month running mean of sunspot number) while the D-region uses R_{12} and F10.7. These sub-models use different functions to approximate the electron density in each region by varying the scale height and tuning the

DUTTA AND COHEN 1 of 12

constant coefficients and offsets based on the available data. The data is sourced from ionosondes, incoherent scatter radar, topside sounders, in situ satellite data, rocket data, and LEO GPS radio occultations, and has been validated using GNSS TEC measurements. However, creating one model that spans such a vast altitude range is a challenge, and the current version of the IRI struggles to properly predict electron densities in the topside as well at high latitudes, even with the addition of physics based topside specific models to the IRI (Migoya-Orue et al., 2013). Recently, a new topside model (referenced as COR2) for the IRI was created, but the current version of the IRI (IRI-2016) still uses the 2007 NeQuick model for the topside. The 2007 NeQuick model represents the topside ionosphere as a semi-Epstein layer with a height-dependent thickness parameter H, and is known to struggle to correctly reproduce high altitude electron densities in the Equatorial Ionization Anomaly (Bilitza & Xiong, 2021; Nava et al., 2008). The COR2 improved model involves the introduction of a correction term based on data from CHAMP, GRACE, Alouette, ISIS, and Swarm data. COR2 performs better than any of the topside options available when running the IRI, namely NeQuick, IRI01-corr, and IRI2001, when validated against satellite data from CHAMP and GRACE as well as Alouette and ISIS topside sounder data. However, the same is not true when validated against Swarm data, where the correction term must be modified to better fit the Swarm data separately from the other data sources. Therefore, there is still a need to create a more robust model of the topside ionosphere.

Many physics-based models make simplifying assumptions that restrict their applicability to one region or section of the magnetosphere/ionosphere/thermosphere system. As such, the coupling interactions between various layers are not so cleanly represented, and are thus not robust to sudden disturbances from high solar activity (Peng et al., 2010). Unfortunately, this means the models do not perform well at the times we need accurate forecasts the most. Shim et al. (2012) compares electron density models using RMS error and prediction efficiency binned by latitude range and true density variability. The study found the IRI to perform better than other model types, including data assimilative models and purely physics-based models. However, the IRI does not perform well in predicting the electron density in the topside of the ionosphere, noted by both the developers of the IRI and validated by them and others via comparison of IRI model output to topside electron density data taken from in situ SWARM, DMSP, and CHAMP measurements (Bilitza et al., 2006; Pignalberi et al., 2018; Themens et al., 2019). We focus here on development of a standalone topside ionospheric electron density model to advance our overall ionospheric modeling capabilities. Prior work suggests combining ionosonde measurements with satellite data to develop better models of the topside ionosphere (Liu et al., 2014). The reason for the relatively high error of the topside in the IRI model is likely related to the relative lack of information that can be inferred from the ground. By creating a machine learning model trained on satellite data, we can better complement and supplement the IRI than other current topside modeling efforts. A multilayer neural network (NN) with many hidden nodes has been applied to predict electron density in the topside ionosphere and plasmasphere in a combined model using data from the Hinotori, Akebono, and Arase satellites (Watanabe et al., 2021). A NN has also been used to predict future electron densities encountered by a LEO satellite in orbit using data from CHAMP (Pérez et al., 2014). DMSP data has been used to predict total electron energy flux using a NN (McGranaghan et al., 2021). Finally, Bortnik et al. (2016) focused on predicting global plasma density in the magnetosphere using a NN. Thus, applying a NN to satellite data to create a better model of an unknown quantity in the space environment is a well-established technique.

The DMSP alone has topside electron density data from 1988 to the present from the Special Sensor-Ions, Electrons, and Scintillation (SSIES) instrument on board each satellite. With a total of 139 satellite-years of useable data through 2019, the modeling problem is a strong candidate for the application of machine learning (ML) techniques. ML allows for model creation with fewer assumptions, since the coupling to other portions of the space weather system is empirically defined, whereas a least squares regression or other curve fitting technique would restrict the relationship based on a chosen parametrization. Additionally, an ML model automatically includes nonlinear dependencies. Therefore, we developed a NN that is trained on existing electron density data to create a model that can nowcast the electron density at any location and time, given the values of global indices F10.7, average interplanetary magnetic field (IMF), and Kp. In this paper, we outline the sources of data used, the feature selection process, and the model architecture selected, ending with a discussion of our results via comparison of the model's performance to that of the IRI, using DMSP data not used in training and DEMETER ISL data for in situ ground truth measurements of the electron density in the topside of the ionosphere. While the IRI uses DMSP data to tune the parameters of its auroral boundary model, the data is not used for development of a topside electron density model. DMSP data is geographically sparse, that is, only *N* geographically electron

DUTTA AND COHEN 2 of 12

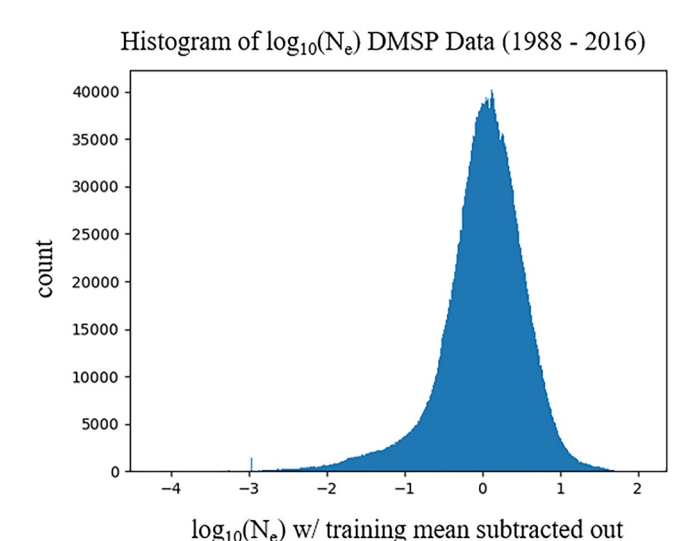


Figure 1. Histogram showing distribution of $\log_{10}(N_e)$ with mean value subtracted out. Data from 1988 to 2011 was used in training, and 2012–2016 for validation, leaving 2017–2019 for testing.

density measurements exist in the DMSP data set at a given time, where N is the number of satellites operational at that time. We posit that this geographically sparse but temporally rich data set is better suited to training a NN to make global electron density predictions. In our conference paper Dutta and Cohen (2021), we presented interim/preliminary results about our machine learning model of the topside ionosphere. The model has since been retrained with an improved set of input features, which performed better on testing data (correlation coefficient up from 0.73 to 0.87). In addition to that and a more complete and detailed description of the technique, our paper here also includes model performance based on data from the DEMETER ISL instrument and detailed analysis comparing the NN to the IRI.

2. Data Preparation

A NN functions well when trained on reliable and consistent data, that is, without contaminated or missing data. Even a sophisticated network architecture will struggle to make a good predictor when trained on bad data. We restrict our focus to 12 out of the 14 DMSP satellites that have been operational to date (DMSP-8 through 19). The first 2 satellites did not record electron density data. The earliest useable data are from 1988, providing over 30 years (139 satellite-years) worth of data to train and/or test our model upon through 2019. The instrument used by all the DMSP satellites to collect

electron density data was the SSIES, which consists of a Langmuir Probe and an ion sensor. The data was sampled once a second and is classified as NASA Level 1 data with no quality flags. We now present our data pre-processing steps.

First, we remove any DMSP data points where the recorded electron density was undefined. We also removed data points from which any of the input data was not recorded properly. On examination of the possible inputs to the model, we found that some earlier values (occurring in 1988–1989) of IMF were corrupted, so those data points were eliminated. Further discussion on the possible model inputs can be found in the Feature Selection section. Next, we examined the distribution of electron densities obtained. The distribution of electron densities sampled along satellite paths of the DMSP appears to be a normal distribution with a left tail skew as seen in Figure 1. Earlier satellites (F08—F15) recorded a few outlier electron densities as low as 106 m⁻³, while more recent satellites (F16—F19) recorded a few outlier electron densities higher than 10¹² m⁻³. The bulk of data lies between 107 and 1012 electrons/m3, and Figure 3 highlights the outlier values. The location of the bulk of data can be seen visually in Figure 2, which shows a histogram of $\log_{10}(N_e)$ in m⁻³ for each DMSP satellite. There were 12 satellites polar orbiting the Earth for anywhere from 2 to 5 years each. We chose to limit our training and testing data electron densities to be between 107 and 1012 electrons/m3 by ignoring data outside of that range, since the values above and below those boundaries are tied to specific satellites, and are unlikely to be indicative of actual electron density values. The figure also demonstrates that some satellites have produced more data than others. Figure 4 plots DMSP data solar local time distributions, one histogram for each satellite, similar to Figure 2. The solar local time of a data point was computed from the UTC time and geographic longitude of data collection using the following formula where UTC is expressed in seconds after midnight and longitude is expressed as an angle between 0 and 360°:

Solar Local Time =
$$\left(\text{UTC} + \frac{\text{longitude} * 24}{360} \right) \mod 24$$

While all of the histograms are bimodal with peaks around 6:00 and 18:00, the satellites collected data at most solar local times, so a NN trained on this data set has been exposed to almost all times of day. Figure 5 depicts DMSP data solar local time distributions by satellite, but restricted to low latitudes. Between midnight and 2, there is no data, but the NN has still been trained on data that covers most solar local times at most latitudes.

In order to validate the model developed, comparisons were made not only to DMSP data not used in model training, but also to the Langmuir Probe Instrument (ISL) aboard the DEMETER satellite (Lebreton et al., 2006).

DUTTA AND COHEN 3 of 12

15427390, 2022, 9, Downloaded from https://agupubs.onlinelibrary.wiley.com/doi/10.1029/2022SW003134 by Georgia Institute Of Technology, Wiley Online Library on [04/01/2023]. See the Term

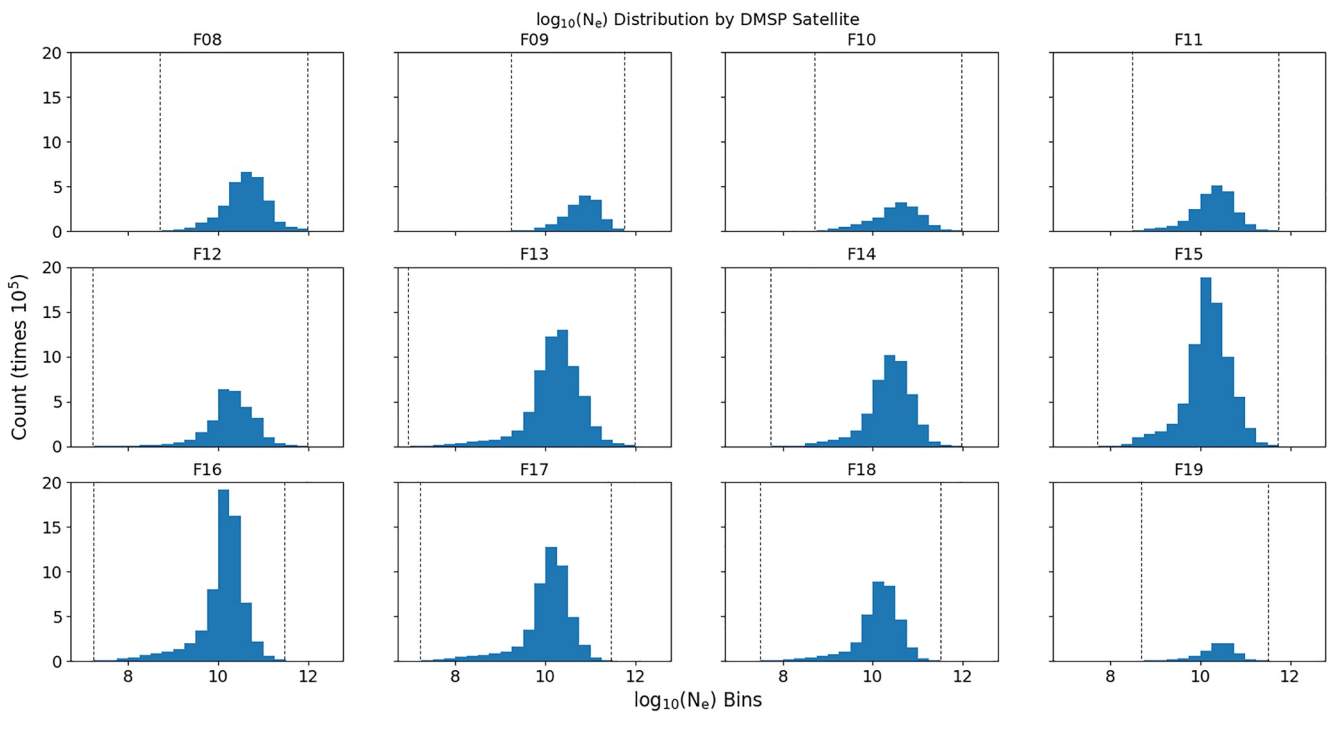


Figure 2. All $\log_{10}(N_e)$ data in histograms by Defense Meteorological Satellite Program satellite number. Satellites were named with the letter F followed by a number. The pair of dotted lines on each panel depict the left and right edges of each histogram. The earlier satellites recorded lower electron densities than the later ones.

DEMETER operated from 2004 to 2010, but the measurements used here are from the earlier months of the satellite's operation when it orbited at an altitude of 710 km, not too far below that of the DMSP satellites (Parrot, 2002). Beyond this date DEMETER's altitude was lowered to 660 km where a direct comparison to DMSP is no longer accurate. This provides a bit over a year of data from July 2004 until December 2005. We note that while the model was trained on a time period that covers the time period of DEMETER data, the DEMETER satellite was at a different location than any of the DMSP satellites at that time, and the data was also collected using a different instrument (DMSP's SSIES vs. DEMETER's ISL), so reporting model results on DEMETER data is still useful, especially when testing is also performed using DMSP data from time periods not trained or validated on.

Figure 6 is a histogram of the altitude of the model training data. The DMSP satellites orbit at about 850 km altitude, but over the lifetime of a satellite, it may drift to a lower altitude while the instruments continue to collect data. The data used for training ranges largely in altitudes of 820–880 km, and we would expect the model to perform particularly well in this altitude range. In order to increase this range, satellite data from other altitudes must be used in training.

3. Feature Selection

Input features to the NN include location (latitude, longitude, altitude, magnetic local time, solar zenith), and global geomagnetic indices relating to different latitudes of the topside ionosphere. The full list of model inputs ultimately chosen is provided in the caption to Figure 7. We used F10.7, Kp, average IMF, and location features including latitude, longitude, and altitude. Longitude and MLT were included as sine and cosine to account for the wrapping around of those features, so that longitude 359° would be adjacent to 0° longitude. Determining the best combination of global indices required experimentation. Using readily available data from NASA OMNIWeb, the index features investigated were 3 hr Kp*10, hourly average IMF, hourly DST, daily F10.7, daily sunspot #R, hourly Sym-H, and daily Lyman- α . The IMF directly impacts the magnetosphere and plasmasphere, which are coupled to the polar ionosphere. Kp and DST both encode information about perturbations of the Earth's magnetic field and are thus likely to provide information about the mid-latitude ionosphere. F10.7 and sunspot number are indicators of the phase of the solar cycle. The index values to use were experimentally determined by

DUTTA AND COHEN 4 of 12

15427390, 2022, 9, Downloaded from https://agupubs.onlinelibrary.wiley.com/doi/10.1029/2022SW003134 by Georgia Institute Of Technology, Wiley Online

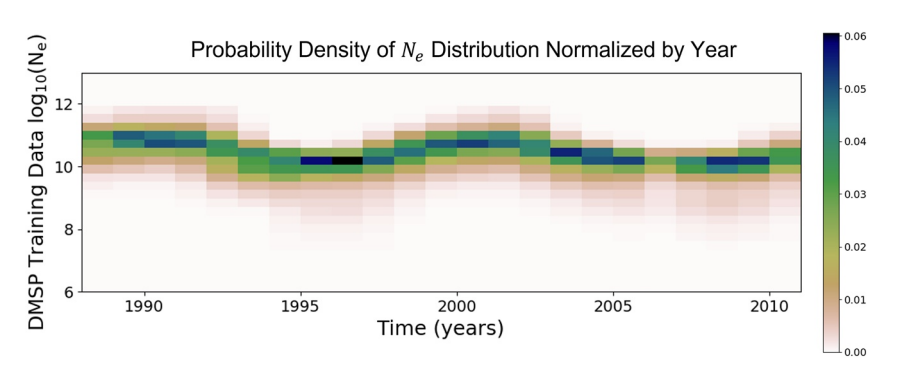


Figure 3. Probability Density of $\log_{10}(N_e)$ training data (1988–2011) from used from Defense Meteorological Satellite Program.

testing various possible combinations and seeing which one performs the best on a testing set of data. Best performance was taken to be the highest correlation coefficient between ground truth DMSP data and NN prediction. For hourly indices, the past 24 hr were used, and for daily indices, the past 7 days were used. Since the model is a nowcaster, these ranges are inclusive of the time we are trying to predict. For example, if we want to predict the electron density at a given location at 13:00 UTC on 08 March 2021, the daily values of F10.7 used are from 02 to 08 March inclusive, the 24 hourly values of IMF used are from 14:00 UTC 07 March 2021 to 13:00 08 March 2021 inclusive, and the 8 hourly values of Kp*10 used are from 16:00 UTC 07 March 2021 to 13:00 UTC 08 March 2021 inclusive. We note that Kp*10 is averaged over three hours, so the value at 13:00 UTC March 08 is actually an average over 12–14:00 UTC. To start, seven models were trained on 22 years of DMSP data, from 1988 to 2011, each with one of the aforementioned index features and all of the location features. The index corresponding to the model that performed best on DMSP data from 2012 to 2016 is saved, and six new models are trained with the winning index feature and one of the remaining six index features. This process was continued

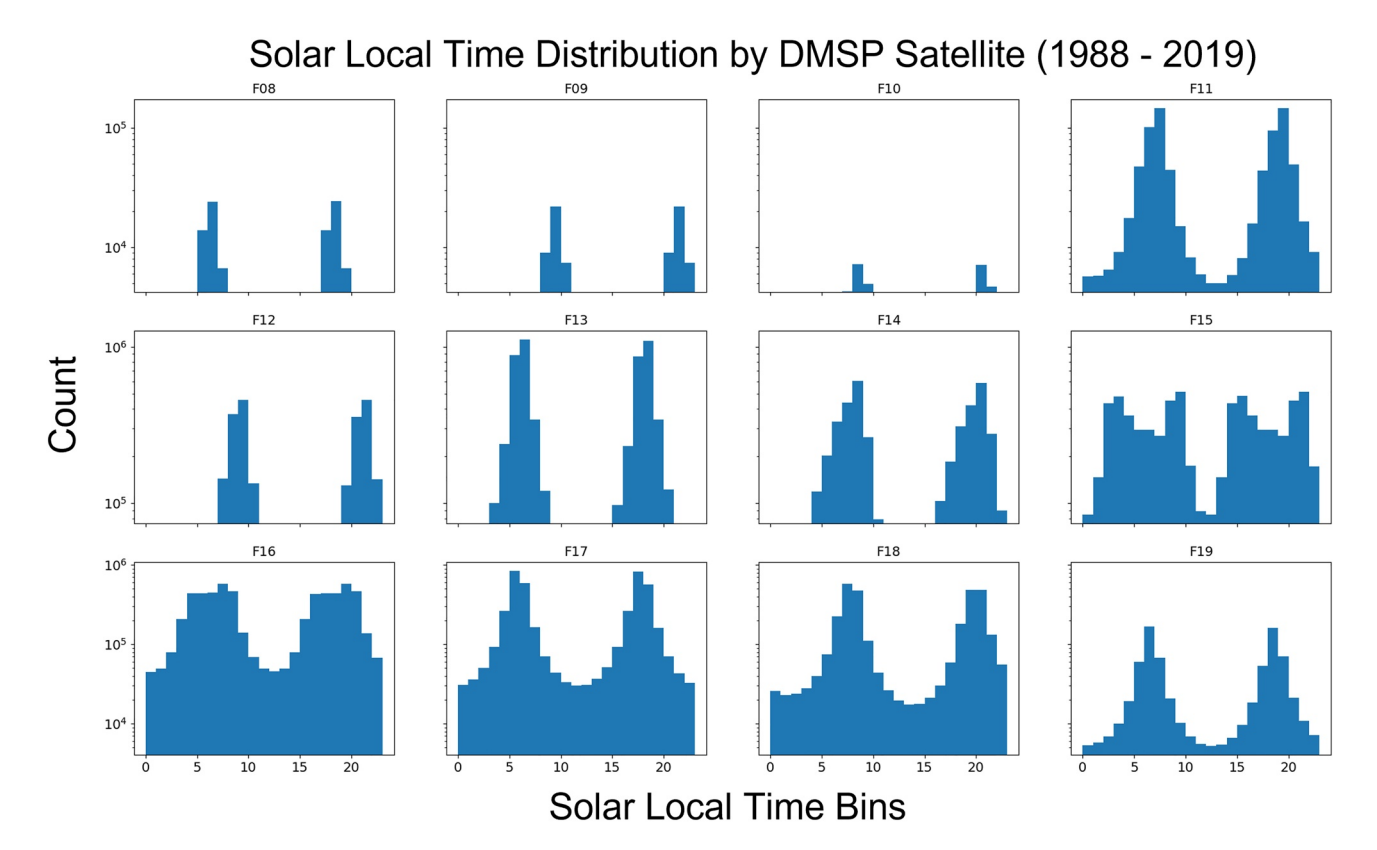


Figure 4. All Defense Meteorological Satellite Program data in histograms by Solar Local Time. Satellites were named with the letter F followed by a number.

DUTTA AND COHEN 5 of 12

15427390, 2022, 9, Downloaded from https://agupubs.onlinelibrary.wiley.com/doi/10.1029/2022SW003134 by Georgia Institute Of Technology, Wiley Online Library on [04/01/2023]. See the Terms

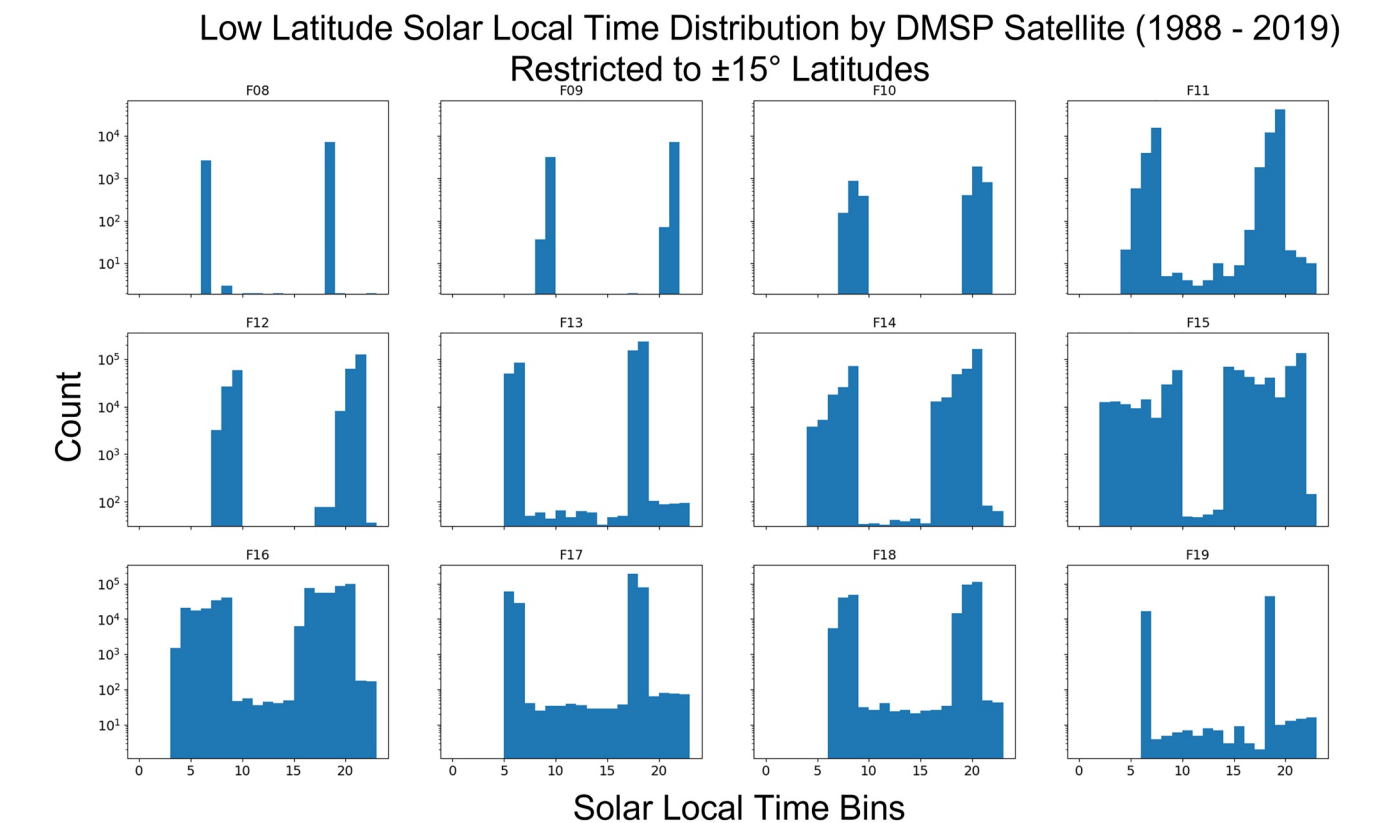


Figure 5. Low latitude $(\pm 15^{\circ})$ Defense Meteorological Satellite Program data in histograms by Solar Local Time. Satellites were named with the letter F followed by a number

until correlation coefficient scores stopped improving. After empirically testing multiple combinations of input features, we settled on using past values of IMF, Kp, and F10.7, which cover the polar region, the mid-latitude region, and the solar cycle respectively.

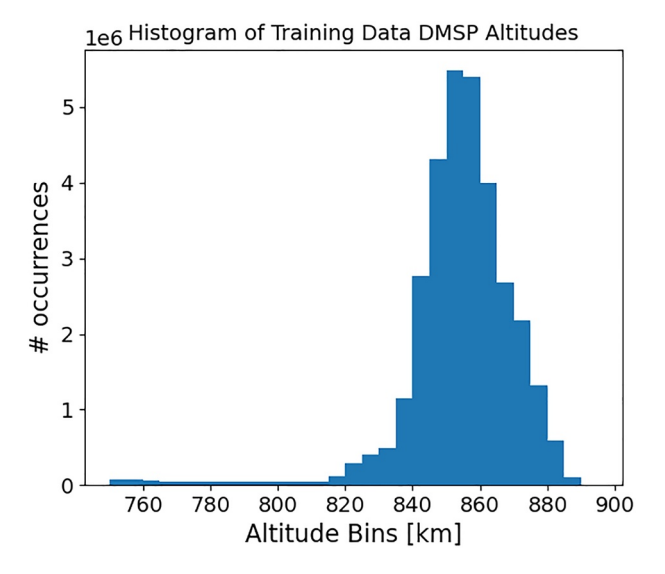


Figure 6. Histogram of training data altitudes. Defense Meteorological Satellite Program satellites mostly collected data around 850 km altitude, with the bulk of the data collected between 820 and 880 km altitude.

4. Model Architecture

A single satellite provides the electron densities at a single location at a single time, with the satellite moving at ~7 km/s in low Earth orbit. However our goal is to be able to predict the electron density within a portion of the topside at any latitude and longitude within the altitude range. Bortnik et al. (2016), which focused on predicting global plasma density in the magnetosphere, achieve this by using a fully connected NN, using location features and global geomagnetic index values to provide the NN with a sense of time. Traditional forecasting or nowcasting problems are often solved with Recurrent Neural Networks. Specifically, Long Short Term Memory (LSTM) networks are used to learn both long range and short range patterns, or contexts, that occur within a system Sherstinsky (2018). However, these networks rely on perfect prior information of the quantity being predicted over the entire spatial model domain. For example, if an LSTM network were to be used to predict the electron density at all coordinates in the topside of the ionosphere, we would need access to the prior electron density at all of those coordinates over a variety of times, which we do not have, since the electron density at altitudes above 300 km require in situ measurements. Instead, we have spatially sparsely sampled data from satellites orbiting at such a high altitude, which provide the electron density at a new location every second as the satellite

DUTTA AND COHEN 6 of 12

and-conditions) on Wiley Online Library for rules of use; OA articles are governed by the applicable Creatiw

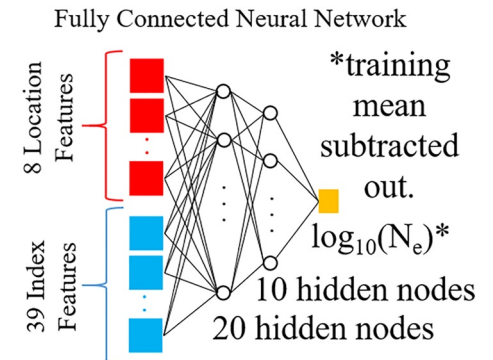


Figure 7. Model architecture used to predict ionospheric electron density. The eight location features are sin/cos of MLT, geographic latitude, sin/cos of geographic longitude, altitude, magnetic latitude, and solar zenith angle. The prior index values used are daily F10.7 (7 values over 7 days), 3 hr Kp (8 values over 24 hr), and hourly average interplanetary magnetic field (24 values over 24 hr).

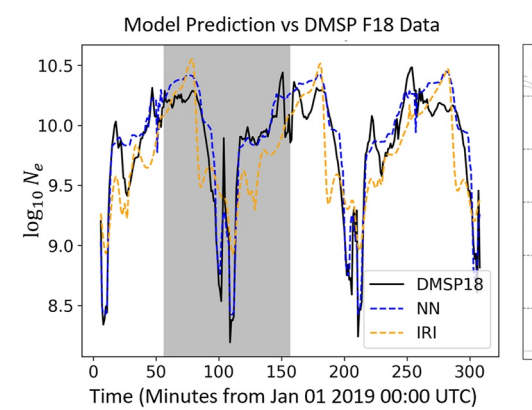
orbits the Earth. Figure 7 depicts the model architecture chosen to accommodate the available data. The red blocks represent the eight features that encode the location of the desired prediction, specifically sin/cos of MLT, geographic latitude, sin/cos of geographic longitude, altitude, magnetic latitude, and solar zenith. The blue blocks represent the index features used to encode the time and the associated solar activity at that time, specifically the past seven daily values of F10.7, the past 8 3-hourly values of Kp*10, and the past 24 hourly values of average IMF. As noted in the Feature Selection section, the time periods used include the time of prediction, making this model a nowcaster.

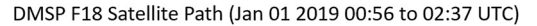
To the extent that the topside ionospheric electron density can be predicted with only knowledge of these features, and assuming we have sufficient data, the machine learning approach should be able to infer the relationship even if complex, discontinuous, or nonlinear. To the extent that the topside ionospheric electron density is chaotic even with knowledge of the global drivers, the model will essentially reduce itself toward a climatological model.

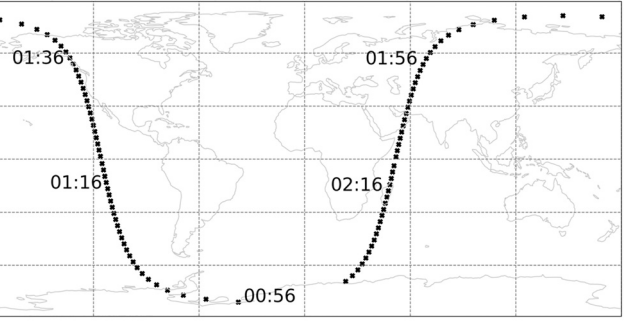
The model is a fully connected NN, so all of these nodes have a weight associated with the next set of 20 hidden nodes, and those 20 hidden nodes have

a weight associated with the next set of 10 hidden nodes, which each have a weight that is associated with the output node, or the electron density prediction. The exact values for the weights are set via the NN training process. We elect to predict $\log_{10}(N_e)$ with the training mean $\log_{10}(N_e)$ subtracted out so that the NN is predicting a value that does not vary by orders of magnitude and is centered about 0, both of which make the training process more efficient. In order to train, the model must have an loss function (here, we use mean square error) associated with it which it seeks to minimize over all training data, so dealing with the error of the exponent is more computationally manageable than the error of the actual electron density values.

The left panel of Figure 8 depicts the NN and IRI predicted electron densities along with the true densities measured by a DMSP satellite over a 300-min period, and the gray area corresponds to the satellite pass in the right panel. The NN appears to more closely follow the DMSP data readings than the IRI, including the double minimum in electron density observed by the north pole. The satellite for this plot was chosen randomly, and this time was chosen since it is at the beginning of a year in our test data set and is convenient to plot, but better performance by the NN versus the IRI is seen throughout the datasets used, as suggested by the correlation coefficients







Path Depicted Here Corresponds to Grey Area in Time Series Panel.

Figure 8. Left panel: 5-hr (300 min) sample of Neural Network and International Reference Ionosphere (IRI) nowcasts of $\log_{10}(N_e)$ compared to actual $\log_{10}(N_e)$ values reported by a Defense Meteorological Satellite Program (DMSP) satellite along its path (Satellite F18 from 01 January 2019). The black curve is the satellite reading, the blue dashed curve is the neural network (NN) prediction, and the orange dashed curve is the IRI prediction. The gray area corresponds to the satellite pass depicted in the right panel. Notice that the NN more closely follows the dips in electron density over the satellite path compared to the IRI, including the double minimum in electron density observed by the satellite around the north pole. Right Panel: One 101 min DMSP F18 satellite pass from 01 January 2019 00:56-02:37 UTC, corresponding to the gray area in the left panel. The satellite starts near the south pole and passes by the north pole in the middle of the pass, which is where the DMSP observes a double minimum in the electron density.

DUTTA AND COHEN 7 of 12

com/doi/10.1029/2022SW003134 by Georgia Institute Of Technology, Wiley Online Library on [04/01/2023]. See the

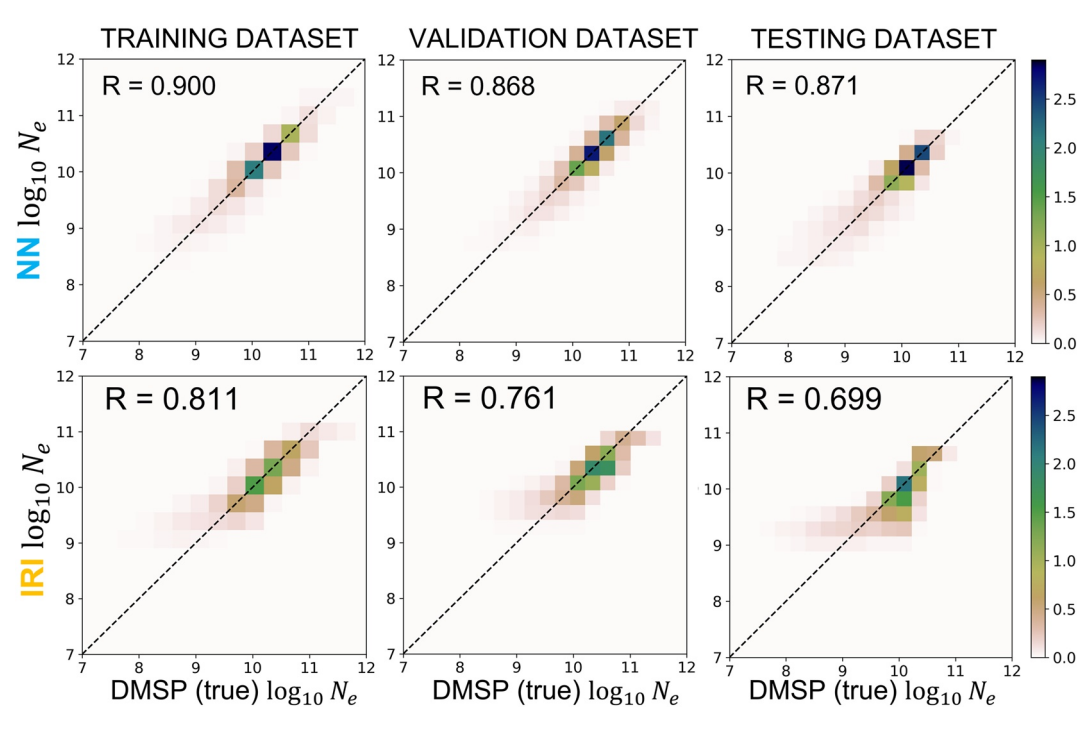


Figure 9. Gaussian Kernel Density Plots comparing results on the training data set (Defense Meteorological Satellite Program (DMSP) 1988–2011) validation data set (DMSP 2012–2016), and testing data set (DMSP 2017–2019) correlation coefficients. The top row uses the Neural Network (NN) to make predictions, while the bottom row uses the International Reference Ionosphere (IRI) to make predictions, and the NN outperforms the IRI on all three datasets.

and plots in Figure 9. Upcoming work includes improved testing performance via modified model inputs, training with synthetic data, and combining the ML model with existing physics-based models.

5. Model Training

The model architecture succeeds at piecing together the complete response of the ionosphere by identifying nonlinear patterns in the evolution of the electron density. To understand how the model converts the DMSP measurements into a complete predictor, consider the following thought exercise. On a given day, the recent kp and solar wind trends are known, but we have data only for the location where the satellite happened to pass on that day. However, it is possible that a similar progression of kp and solar wind trends occurred in the past, when the satellite was in a different location. If there is any consistency in the ionospheric response to a certain progression of kp and solar wind, then the model will eventually learn this pattern. However, the model also needs to learn what patterns actually repeat and are predictable, and what is simply noise. The process of collecting all the historical data and inferring this (nonlinear) pattern is known as training. In a typical machine learning training regimen, a small fraction of the data is set aside to test the model. Here, 80% of the data was used to quantify the nonlinear patterns, and the model was then validated by the remaining 20% of the data. If the model overfits, meaning it fits the model to noise in the training data, then the application of the trained model to the test data set will fail with higher error. This allows the algorithm to adapt, essentially filtering out the variations from noise a leaving only the variations that are reliable and repeatable. This is achieved through an iterative and adaptive process that tunes the model trained on the 80% so that it works very effectively on the 20%.

To train the NN, we first constructed the network in Python 3.7 using torch.nn, a component of the open source PyTorch package. Specifically, the model uses torch.nn.Sequential() with three Linear layers separated by Sigmoid activations, the output of which is passed through a final Linear layer and a Flatten layer. The Flatten layer merely ensures the output of the model is a 1D array containing one value, as opposed to a 2D array containing one value, and does not change the numerical output from the Linear layer. Training was completed using the ignite Python library, a high-level wrapper that makes torch easier to read. The loss function used was Mean Squared Error, and the optimizer used was Root Mean Squared Propagation. We trained

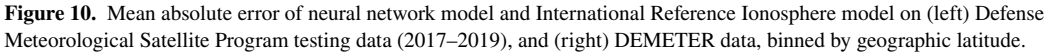
DUTTA AND COHEN 8 of 12

DMSP Testing Data - Abs Err. By Lat

>75 >60 >45 >30 >15 >0 >-15 >-30 >-45 >-60 >-75 <-75

Bin Mean Lat Value

15427390, 2022, 9, Downloaded from https://agupubs.onlinelibrary.wiley.com/doi/10.1029/2022SW003134 by Georgia



NN

IRI

the model on DMSP data from 1988 to 2011. The model was trained until the performance (mean squared error) on validation data (years 2012–2016) stopped improving by setting the maximum number of epochs to be large (1,000), and setting the patience (number of epochs to wait for an increasing error to start decreasing again) to 15, ultimately returning the model trained to the point it performed best on the validation data, preventing overfitting. In the top row of Figure 9, the correlation coefficient between the NN output highlighted in this paper on training, validation, and testing datasets is provided. We obtain a correlation coefficient of 0.90 on training data, versus 0.87 on validation data, and 0.87 on testing data. The bottom row of Figure 9 provides the performance of the IRI on the same datasets, which is worse than the NN on all three datasets. Specifically, the IRI obtains correlation coefficients of 0.81, 0.76, and 0.70 on the training, validation, and testing datasets.

6. Results

4.5

4.0

3.5

3.0

2.5

2.0

1.5

1.0

MAE [$\times 10^{10} e^{-}/m^{3}$]

After completing the training process, the NN's performance was tested using 1. DMSP data not used in the training or validation process (plots here are from DMSP years 2017-2019) and 2. DEMETER Survey data. As noted in the feature selection section, the NN used a combination of location information and global index values to make predictions. We present the mean absolute error (MAE) of a model (NN or IRI) binned by the average index value found in the time leading up to the desired prediction time, and the same errors binned by latitude. The results depicted in the plots for Kp in Figure 11 are a proxy for results when binning across any of the three index values used. A similar pattern is found when binning across IMF or F10.7. The NN performs better than the IRI across all geomagnetic conditions when the ground truth data comes from a DMSP satellite, but the NN only does better for quiet geomagnetic conditions when the ground truth data is sourced from DEMETER. The main differences between DMSP and DEMETER data is the time period the data is sourced from, and the altitude at which the data was collected. The DEMETER data is from July 2004 to December 2005, a period that had a higher level of solar activity than the time period the DMSP data is from (2017 to 2019). However, the NN model was trained on DMSP data collected at a mean altitude of 850 km, while DEMETER data was collected at 700 km. Then the DMSP test data set is a fair test of the NN, while the DEMETER test data set presents the NN a challenge due to its more volatile geomagnetic conditions and its lower altitude. Despite those challenges from the DEMETER test data set, the NN still outperforms the IRI in quiet conditions. Figure 12 is a histogram of the Kp*10 value associated with all DMSP training data. It is unsurprising that the NN performs considerably better at Kp values lower than 4.5, and worse at values higher than that, when the majority of training data is from the lower Kp quiet-time conditions. In Figure 10, we binned the MAE by geographic latitude. We see a similar pattern in Figure 10 as in Figure 11, where here the NN outperforms the IRI across all latitudes when the test data set comes from DMSP, but the NN only outperforms the IRI in the mid-latitudes when the test data set comes from DEMETER.

The plots in Figure 13 depict the IRI model Mean Percent Error (MPE) next to the NN model MPE using DEME-TER data as ground truth. The 2016 IRI was run with the NeQuick topside model, and IRI provided solar index values were used. These plots provide both an intuitive understanding of the satellite coverage of the DEMETER

DUTTA AND COHEN 9 of 12

15427390, 2022, 9, Downloaded from https://agupubs.onlinelibrary.wiley.com/doi/10.1029/2022SW003134 by Georgia Institute Of Technology, Wiley Online

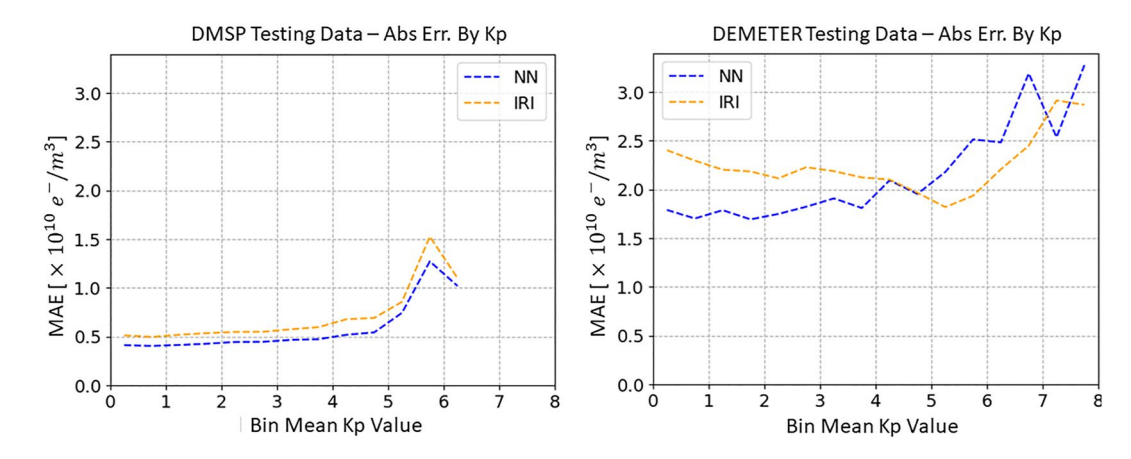


Figure 11. Mean absolute error of neural network model and International Reference Ionosphere model on (left) Defense Meteorological Satellite Program testing data (2017–2019), and (right) DEMETER data, binned by Kp index.

mission, and also depict the better performance of the NN about the magnetic equator. In contrast, the IRI model produces distinct bands of poorer performance about the magnetic equator.

7. Discussion

The goal of this paper was to apply machine learning techniques to the abundance of available electron density data to create a model of the topside of the ionosphere. While the data is abundant over time, it is spatially sparse, and so a NN approach was required as opposed to a long short-term memory network. The network created is fully connected, and has two hidden layers with sigmoid activation functions between the layers, and obtained a correlation coefficient of 0.87 on DMSP testing data (2017–2019). Currently, prior values of F10.7, average IMF magnitude, and Kp*10 are used to provide information about solar activity and how it couples to the ionosphere. When presenting MAE results on the DMSP test data set and the DEMETER test data set, we capture model behavior in two slightly different domains. DMSP data was collected at a mean altitude of 850 km, while the DEMETER data was collected at a mean altitude of 700 km. The NN was trained on DMSP data, and outperforms the IRI when compared to data collected from the DMSP across all geomagnetic conditions (Kp) and all latitudes.

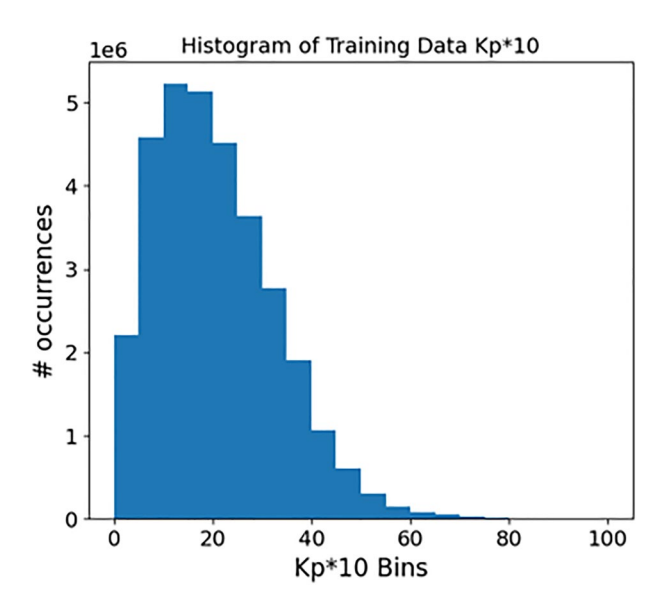


Figure 12. Histogram of Kp*10 value associated with each Defense Meteorological Satellite Program training data point.

When we make comparisons between the NN and the IRI on the DEMETER test data set, we find that the NN outperforms the IRI during quiet solar conditions, with Kp < 5, as well as at mid-latitudes. Due to the lower altitude of the DEMETER satellite the NN performance depicted on DEMETER data is pessimistic in that the model is pushed outside of the regime it was trained in, so strong performance even in calm geomagnetic conditions and about the mid-latitudes is noteworthy.

8. Future Work

Upcoming work includes improved testing performance via modified model inputs, training with synthetic data, and combining the ML model with existing physics-based models. An example of modifying the model inputs would be retraining the model with the z-component of the Earth's magnetic field as opposed to the average IMF value, which may make the NN a better predictor of electron densities in the polar region. As seen in Figure 12, much of the data the NN is currently trained on is from times with low solar activity, so the creation of synthetic data that resembles the existing high solar activity data and retraining the model with a more even balance between quiet time and storm time data may also improve the ML model. Finally, models like the IRI and E-CHAIM have their own strengths and weaknesses, so ensembling the outputs of those model with the output of the NN with an overarching NN

DUTTA AND COHEN 10 of 12

15427390, 2022, 9, Downloaded from https://agupubs.onlinelibrary.wiley.com/doi/10.1029/2022SW003134 by Georgia Institute Of Technology, Wiley Online Library on [04/01/2023]. See

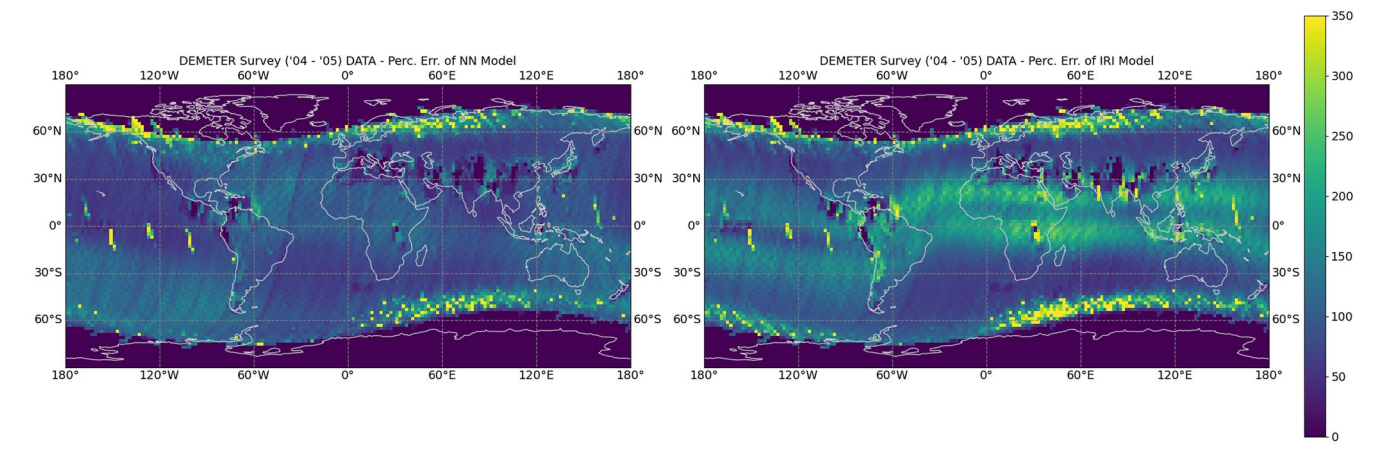


Figure 13. Mean Percent Error of neural network model and International Reference Ionosphere model on DEMETER data, overlaid on map labeled with geographic latitude and longitude.

could combine the strengths of all three while minimizing their weaknesses. After making all of these improvements to the model, the model can be used to then create an ionospheric electron density simulator and forecaster, given prior or predicted values of the solar indices used as inputs to the model.

Data Availability Statement

We accessed the Defense Meteorological Satellite Program data set via the CEDAR Madrigal Database available at http://cedar.openmadrigal.org/ from Doherty (2019). Solar Index values were accessed via NASA OMNIWeb Data Explorer available at https://omniweb.gsfc.nasa.gov/form/omni_min.html and https://omniweb.gsfc.nasa.gov/form/dx1.html for high resolution (minute cadence) and low resolution (hourly or daily) data, respectively, from Papitashvili et al. (2020a, 2020b). DEMETER ISL data were accessed via the CDPP Data Server available at https://cdpp-archive.cnes.fr/ from CDPP (2020). A static version of our trained model and instructions to use it to create topside electron density predictions is available from Dutta (2022) at https://doi.org/10.5281/zenodo.6471156.

Acknowledgments

This work is supported by the Defense Advanced Research Projects Agency through US Department of the Interior award D19AC00009 to the Georgia Institute of Technology.

References

Bilitza, D. (2018). IRI the international standard for the ionosphere. Advances in Radio Science, 16, 1–11. https://doi.org/10.5194/ars-16-1-2018
Bilitza, D., Altadill, D., Truhlik, V., Shubin, V., Galkin, I., Reinisch, B., & Huang, X. (2017). International reference ionosphere 2016: From ionospheric climate to real-time weather predictions. Space Weather, 15(2), 418–429. https://doi.org/10.1002/2016sw001593

Bilitza, D., Reinisch, B. W., Radicella, S. M., Pulinets, S., Gulyaeva, T., & Triskova, L. (2006). Improvements of the international reference ionosphere model for the topside electron density profile. *Radio Science*, 41(5), RS5S15. https://doi.org/10.1029/2005rs003370

Bilitza, D., & Xiong, C. (2021). A solar activity correction term for the IRI topside electron density model. *Advances in Space Research*, 68(5), 2124–2137. https://doi.org/10.1016/j.asr.2020.11.012

Bortnik, J., Li, W., Thorne, R. M., & Angelopoulos, V. (2016). A unified approach to inner magnetospheric state prediction. *Journal of Geophysical Research: Space Physics*, 121(3), 2423–2430. https://doi.org/10.1002/2015JA021733

CDPP Plasma Physics Data Center. (2020). DEMETER Mission ISL [Dataset]. https://cdpp-archive.cnes.fr/

Council, N. R. (2008). Severe space weather events: Understanding societal and economic impacts: A workshop report. The National Academies Press. Retrieved from https://www.nap.edu/catalog/12507/severe-space-weather-events-understanding-societal-and-economic-impacts-a

Doherty, P., & Institute for Scientific Research. (2019). Defense Meteorological Satellite Program [Dataset]. From CEDAR Madrigal Database. Retrieved from cedar.openmadrigal.org

Dutta, S., & Cohen, M. B. (2021). Modeling electron density in the topside of the ionosphere using machine learning. In 2021 XXXIVth general assembly and scientific symposium of the international union of radio science (URSI GASS). IEEE. https://doi.org/10.23919/ursigass51995.2021.9560493

 $Dutta, S.\ (2022).\ \textit{Topside Ionosphere Electron Density Model}.\ Zenodo.\ https://doi.org/10.5281/ZENODO.6471156$

Lebreton, J.-P., Stverak, S., Travnicek, P., Maksimovic, M., Klinge, D., Merikallio, S., et al. (2006). The ISL Langmuir probe experiment processing onboard DEMETER: Scientific objectives, description and first results. *Planetary and Space Science*, 54(5), 472–486. https://doi.org/10.1016/j.pss.2005.10.017

Liu, L., Huang, H., Chen, Y., Le, H., Ning, B., Wan, W., & Zhang, H. (2014). Deriving the effective scale height in the topside ionosphere based on ionosonde and satellite in situ observations. *Journal of Geophysical Research: Space Physics*, 119(10), 8472–8482. https://doi.org/10.1002/2014ja020505

DUTTA AND COHEN 11 of 12



Space Weather

- 10.1029/2022SW003134
- McGranaghan, R. M., Ziegler, J., Bloch, T., Hatch, S., Camporeale, E., Lynch, K., et al. (2021). Toward a next generation particle precipitation model: Mesoscale prediction through machine learning (a case study and framework for progress). Space Weather, 19(6). https://doi.org/10.1029/2020sw002684
- Migoya-Orue, Y., Radicella, S., & Nava, B. (2013). Comparison of topside electron density computed by ionospheric models and plasma density observed by DMSP satellites. *Advances in Space Research*, 52(10), 1710–1716. https://doi.org/10.1016/j.asr.2013.01.032
- Nava, B., Coïsson, P., & Radicella, S. (2008). A new version of the NeQuick ionosphere electron density model. *Journal of Atmospheric and Solar-Terrestrial Physics*, 70(15), 1856–1862. https://doi.org/10.1016/j.jastp.2008.01.015
- Papitashvili, N. E., & King, J. H. (2020a). "OMNI 1-min Data" [Dataset]. NASA Space Physics Data Facility. https://doi.org/10.48322/45bb-8792 Papitashvili, N. E., & King, J. H. (2020b). "OMNI Hourly Data" [Dataset]. NASA Space Physics Data Facility. https://doi.org/10.48322/1shr-ht18 Parrot, M. (2002). The micro-satellite DEMETER. *Journal of Geodynamics*, 33(4–5), 535–541. https://doi.org/10.1016/s0264-3707(02)00014-5
- Peng, Z., Wang, C., & Hu, Y. Q. (2010). Role of IMFBxin the solar wind-magnetosphere-ionosphere coupling. *Journal of Geophysical Research*, 115(A8). https://doi.org/10.1029/2010ja015454
- Pérez, D., Wohlberg, B., Lovell, T. A., Shoemaker, M., & Bevilacqua, R. (2014). Orbit-centered atmospheric density prediction using artificial neural networks. *Acta Astronautica*, 98, 9–23. https://doi.org/10.1016/j.actaastro.2014.01.007
- Pignalberi, A., Pezzopane, M., & Rizzi, R. (2018). Modeling the lower part of the topside ionospheric vertical electron density profile over the European region by means of swarm satellites data and IRI UP method. Space Weather, 16(3), 304–320. https://doi.org/10.1002/2017sw001790
- Sherstinsky, A. (2018). Fundamentals of recurrent neural network (rnn) and long short-term memory (lstm) network. In *Elsevier "physica D: Nonlinear phenomena" journal, volume 404, March 2020: Special issue on machine learning and dynamical systems.* https://doi.org/10.1016/j. physd.2019.132306
- Shim, J. S., Kuznetsova, M., Rastätter, L., Bilitza, D., Butala, M., Codrescu, M., et al. (2012). CEDAR electrodynamics thermosphere ionosphere (ETI) challenge for systematic assessment of ionosphere/thermosphere models: Electron density, neutral density, NmF2, and hmF2 using space based observations. Space Weather, 10(10). https://doi.org/10.1029/2012sw000851
- Themens, D. R., Jayachandran, P. T., & McCaffrey, A. M. (2019). Validating the performance of the empirical Canadian high Arctic ionospheric model (e-CHAIM) with in situ observations from DMSP and CHAMP. *Journal of Space Weather and Space Climate*, 9, A21. https://doi.org/10.1051/swsc/2019021
- Watanabe, S., Miyoshi, Y., Tsuchiya, F., Kumamoto, A., Kasahara, Y., Matsuoka, A., & Shinohara, I. (2021). Modeling of topside ionosphere and plasmasphere. https://doi.org/10.21203/rs.3.rs-380095/v1

DUTTA AND COHEN 12 of 12